Blue photoluminescence of highly photoexcited rutile TiO_2: Nearly degenerate conduction-band effects

Yasuhiro Yamada[1] and Yoshihiko Kanemitsu[1,2,*]
[1]*Institute for Chemical Research, Kyoto University, Uji, Kyoto 611-0011, Japan*
[2]*Photonics and Electronics Science and Engineering Center, Kyoto University, Kyoto 615-8510, Japan*
(Received 6 June 2010; published 20 September 2010)

We report the observation of blue photoluminescence (PL) from highly photoexcited rutile TiO_2 single crystals at room temperature. Under extremely high-density excitation, we found an anomalous dependence of the PL dynamics and intensity on the excitation density. By considering the nearly degenerate conduction bands of rutile, we revealed that the PL behavior is determined by the electron density in the lower-energy conduction band. The PL decay dynamics is well explained by the simple model involving two-body radiative recombination and three-body Auger recombination processes. We discuss the origin of the blue PL band.

DOI: 10.1103/PhysRevB.82.113103 PACS number(s): 78.55.−m, 72.20.Jv, 78.47.D−

Transition-metal oxides and their heterostructures have attracted a great deal of attention as new device materials due to their wide variety of fascinating and multifunctional properties beyond those of conventional semiconductors. TiO_2 is a wide-gap semiconductor with a band-gap energy of 3.0 eV. From both a technological and a fundamental physics viewpoint, it is one of the most important oxide materials. Due to its large dielectric constant and strong electron-phonon coupling, the anomalous electronic conduction in rutile has been of considerable interest in conjunction with unusual band structures.[1–3] In recent years, increasing attention has been paid to the unique and functional optical properties of TiO_2, as it is used in photocatalysts,[4] transparent conducting materials,[5] and dye-sensitized solar cells.[6] As the characteristics of the photocatalytic reaction and solar-energy conversion are governed by photocarriers, which promote a chemical reaction or generate electric potential, it is important to study the photocarrier dynamics and transport processes. Although extensive time-resolved microwave photoconductivity,[7] transient absorption,[8] terahertz spectroscopy,[9] time-resolved reflectance,[10] and other similar studies have been made, the carrier dynamics, which determines the electronic properties of TiO_2, still remains unclear.

In studying photocarrier dynamics, photoluminescence (PL) spectroscopy is one of the most versatile and commonly used tools. However, no intrinsic PL has so far been reported in rutile TiO_2 bulk crystals at room temperature, except for that due to impurity or defects,[11] and this prevents us from a deep understanding of the photocarrier dynamics of TiO_2 crystals. In this Brief Report, we report the observation of blue PL in highly photoexcited rutile TiO_2 at room temperature. The PL intensity and dynamics depend strongly on the photogenerated carrier density. The PL dynamics is well explained by a simple model involving nonradiative single-carrier trapping, radiative bimolecular recombination, and three-body Auger recombination. However, under extremely high excitation, the excitation-density dependence of the blue PL intensity and dynamics deviates from that expected from the simple rate equation model. This unusual behavior can be explained by considering the nearly degenerate conduction bands of rutile crystals.

We used commercially available nondoped rutile and 0.05 mol % Nb-doped rutile single crystals (Furuuchi Chemical Co.). The faces of the samples, which were 0.5 mm thick, were oriented along the [100] direction. Time-resolved PL measurements were performed using a streak camera and a monochromator. The time resolution of our setup was 40 ps. The excitation light source was an optical parametric amplifier system based on a regenerative amplified mode-locked Ti:sapphire laser with a pulse duration of 150 fs and a repetition rate of 1 kHz. The excitation photon energy was 3.35 eV. The laser spot size on the sample surface was measured carefully using the knife-edge method.

Figure 1(a) shows the time-integrated PL spectrum of the nondoped rutile crystal under an excitation of 4.2 mJ/cm^2. The optical absorption spectrum is also shown in the figure. The PL spectrum has a broad asymmetric peak at around 2.8 eV. We confirmed that the spectrum shape is independent of the excitation photon energy. The large Stokes shift (E_s =0.2 eV) and broad spectral width (full width at half maximum: 0.4 eV) indicate that the localization of photocarriers plays an essential role for the blue PL. This blue PL band is observed only under the intense pulse laser excitation, but no blue PL is observed under weak continuous-wave (cw) excitation. We also observed similar blue PL in electron-doped rutile (Nb: 0.05 mol %) under a relatively low-excitation density of 31 $\mu J/cm^2$, as shown in Fig. 1(b). The blue PL in Nb-doped rutile is observed even under cw excitation. These results indicate that the blue PL in nondoped and electron-doped rutile is related to high-density carriers in the samples.

Figure 2(a) shows the PL decay dynamics monitored at 2.8 eV in nondoped rutile under excitation of 0.22, 3.9, 17, and 33 mJ/cm^2. In nondoped rutile, under a low-excitation density below 0.4 mJ/cm^2, the PL decay dynamics shows a single exponential decay with a time constant of 22 ns. When the excitation density exceeds 0.4 mJ/cm^2, a fast and nonlinear decay component appears. The PL decays faster as the excitation density increases. This suggests that the PL decay dynamics under high density excitation is dominated by nonlinear recombination processes such as nonradiative Auger recombination. The PL decay dynamics in Nb-doped rutile under a weak excitation of 31 $\mu J/cm^2$ is shown in Fig. 2(b). As shown in the inset of Fig. 2(b), the PL intensity of electron-doped rutile shows a linear dependence on the excitation density, I_{ex}, unlike that of nondoped rutile. This indicates that the blue PL in electron-doped rutile originates from

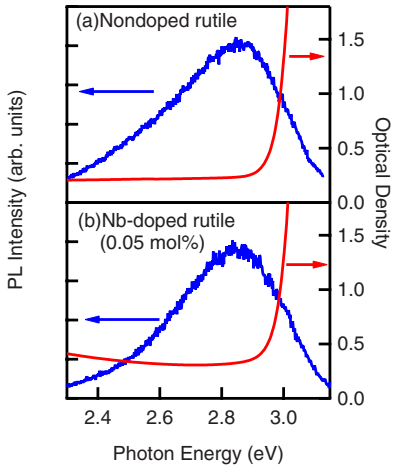

FIG. 1. (Color online) Time-integrated PL and optical density spectra at 300 K in (a) nondoped rutile and (b) Nb-doped rutile (0.05 mol %).

the bimolecular recombination of chemically doped electrons and photoexcited holes, and thus the blue PL is observed even under weak photoexcitation in electron-doped rutile. The PL decay profile shows single exponential decay with a decay time of 9 ns, which is faster than that of the nondoped rutile under weak excitation density, indicating that the Auger recombination of doped electrons and photoexcited holes (electron-hole-electron Auger process) dominates the PL dynamics in electron-doped rutile. The PL decay dynamics is almost independent of the excitation density below 100 $\mu J/cm^2$, where the photocarrier density is much smaller than the doped carrier density.

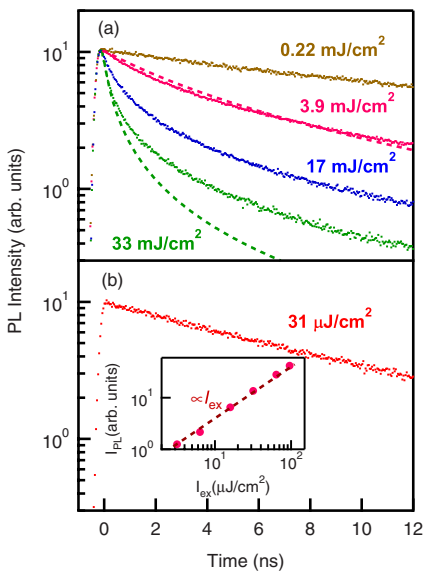

FIG. 2. (Color online) (a) PL decay dynamics of nondoped rutile under the excitation of 0.22, 3.9, 17, and 33 mJ/cm^2 monitored at 2.8 eV. The broken curves show the calculated curves by Eqs. (1a) and (1b) under 3.9 and 33 mJ/cm^2 excitations. (b) PL decay dynamics of Nb-doped rutile (0.05 mol %) under excitation of 31 $\mu J/cm^2$. The inset shows the excitation-density (I_{ex}) dependence of blue PL intensity.

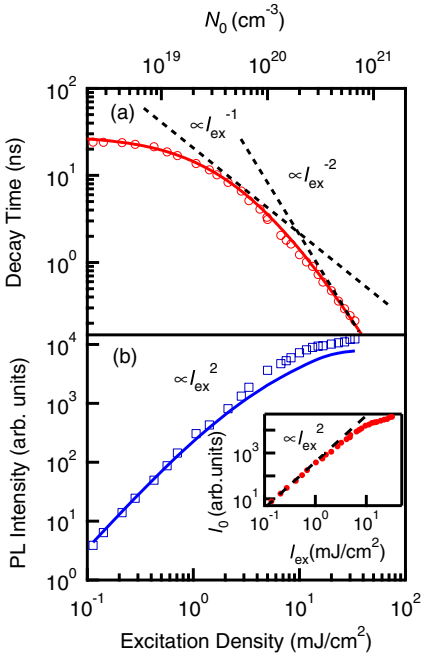

FIG. 3. (Color online) The excitation-density dependence of (a) the decay time and (b) the time-integrated PL intensity in nondoped rutile. The inset shows the excitation-density dependence of the initial PL intensity I_0.

The rate equation for photocarriers in semiconductors is usually described by the following equations:[12–14]

$$\frac{dn}{dt} = -An - Bn^2 - Cn^3, \tag{1a}$$

$$I_{PL}(t) \propto n^2, \tag{1b}$$

where n and $I_{PL}(t)$ are the photocarrier density and PL intensity, respectively. In the Eq. (1a), the first term represents the single-carrier trapping process. The B coefficient is composed of the radiative bimolecular recombination and nonradiative trap-assisted Auger recombination processes. The Cn^3 term represents the nonradiative Auger recombination, which involves the electron-electron-hole and electron-hole-hole processes. Based on the above carrier recombination model, we discuss the blue PL dynamics of rutile. The excitation density dependence of the blue PL intensity and PL decay time in rutile is summarized in Fig. 3. Here, we defined the decay time $t_{1/e}$ by $I_{PL}(t_{1/e}) = I_{PL}(0)/e$, where $I_{PL}(t)$ is the PL intensity at time t. The photogenerated carrier density N_0 is estimated from the incident photon number and the optical absorption coefficient.[15]

Figure 3(a) shows the decay time $t_{1/e}$ as a function of the excitation density. The decay time stays almost constant at around 22 ns below 0.4 mJ/cm^2 and gradually decreases as the excitation density increases. The excitation-density dependence of the PL intensity is shown in Fig. 3(b). Under the low-excitation density (below 3 mJ/cm^2), the PL intensity shows the quadratic dependence on the excitation density, indicating radiative bimolecular recombination of photoexcited electrons and holes. When the excitation density ex-

ceeds 3 mJ/cm^2, the PL intensity starts to saturate. The solid curves in Figs. 3(a) and 3(b) show the result calculated using Eqs. (1a) and (1b) with $A=1.9\times10^7$ s^{-1}, $B=5.3\times10^{-13}$ cm^3 s^{-1}, and $C=1.0\times10^{-32}$ cm^6 s^{-1}. The calculated curve for the decay time almost coincides with the experimental results. However, we find a significant difference between the calculated PL intensity and the experimental result in the high excitation-density region. Moreover, the initial PL intensity I_0 [$=I_{PL}(0)$] as a function of the excitation density is shown in the inset of Fig. 3(b). Whereas the initial PL intensity shows the quadratic dependence on the excitation density below 3 mJ/cm^2, saturation occurs when the excitation density is high. We also plotted the calculated PL decay curves using Eqs. (1a) and (1b) with the above A, B, and C coefficients in Fig. 2(a). The calculated curves show large disagreement with the experimental results under extremely high-density excitation. This behavior is completely different from that of other typical semiconductors such as Si (Refs. 12 and 13) and $SrTiO_3$ (Refs. 14, 16, and 17) and is an essential feature of rutile.

To understand the origin of the anomalous excitation-density dependence of the PL behavior under extremely high-density excitation, we consider the unique band structure of rutile. The optical absorption measurement[18,19] and band calculation[20,21] revealed that rutile is a direct-forbidden gap semiconductor: the direct transition [Γ(conduction band)$\rightarrow\Gamma$(valence band)] is dipole forbidden, and the indirect-allowed transition [M$\rightarrow\Gamma$ (Ref. 20) or R$\rightarrow\Gamma$ (Ref. 21)] is nearly degenerate with the direct-forbidden transition. The energy separation between the direct-forbidden and indirect-allowed transitions is estimated to be 10–50 meV.[19,22,23] This "nearly degenerate band model" has been used to describe the unusual temperature dependence of the conductivity and Hall coefficient in rutile.[24,25] Following the nearly degenerate conduction-band model, the electron distribution between the lower-energy direct band (Γ point) and the higher-energy indirect band (R or M point) states will be strongly dependent on temperature and excitation density. This causes the unusual excitation-density dependence of the PL behaviors in rutile. In our experiment at 300 K [Fig. 3(b)], the PL intensity saturation occurs at around 7 mJ/cm^2, corresponding to a photocarrier density of $N_0=1.4\times10^{20}$ cm^{-3}. For the effective mass of rutile $m^*=7-20m_e$,[25–27] we can obtain the Fermi level $E_F=6-20$ meV from the bottom of the conduction-band edge, following $E_F=\hbar^2(3\pi^2N_0)^{2/3}/(2m^*)$, which is consistent with the energy separation between the direct and indirect bands. Thus, we believe that the carrier distribution in the nearly degenerate conduction bands plays an essential role in carrier recombination dynamics under high-density excitation.

Because the thermal energy is comparable to the energy separation between the lower and higher conduction bands, the carrier recombination process is complicated at 300 K as mentioned above. To clarify the effect of the nearly degenerate conduction bands on PL dynamics we measured the PL spectrum and dynamics at 8 K where electron population in the higher-energy conduction band is negligibly small. We can analyze the PL dynamics at low temperatures without considering thermal population effects.

Figure 4 shows the time-integrated PL spectra in non-

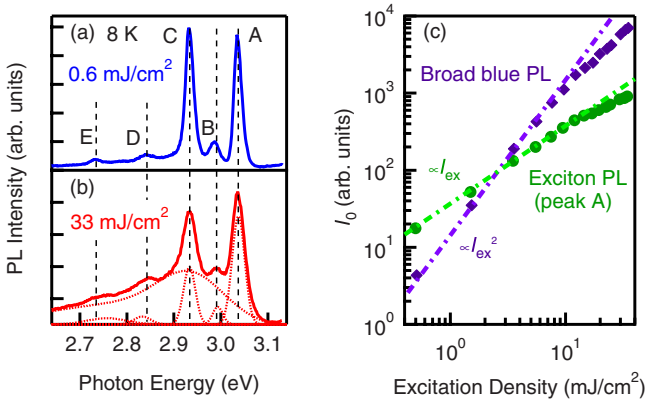

FIG. 4. (Color online) PL spectra of nondoped rutile under (a) 0.6 mJ/cm^2 and (b) 33 mJ/cm^2 excitations at 8 K. (c) The excitation density dependence of the initial PL intensity of broad blue PL and exciton PL (peak A).

doped rutile under excitations of (a) 0.6 mJ/cm^2 and (b) 33 mJ/cm^2 at 8 K. We observed several PL lines (A–E) under a low-excitation density of 0.6 mJ/cm^2. Amtout and Leonelli[19] have assigned the peak A to $2p_{xy}$ direct exciton PL and peaks B–E as phonon replicas of the Γ_5 symmetry of $1s$ excitons. However, under high excitation (33 mJ/cm^2), a broad PL component appears in addition to the sharp PL lines. As is evident from the decomposed spectra shown in Fig. 4(b) (dotted curves), the broad blue PL also appears at low temperatures. We have confirmed that the broad blue PL appears under high-density excitation in the temperature range from 8 to 300 K. The peak energy and spectral width of the broad PL show no dependence on the temperature and the photocarrier density.

The excitation-density dependence of the broad blue PL intensity and exciton PL (peak A) is shown in Fig. 4(c), where the broad blue PL and exciton PL are monitored at 2.65 eV and 3.05 eV, respectively. Under low-excitation density (below 10 mJ/cm^2), the broad blue PL and exciton PL intensity show quadratic and linear dependences on the excitation density, respectively. When the excitation density exceeds 10 mJ/cm^2, both broad blue and exciton PLs saturate. This observation suggests that under extremely high-density excitation hot electron-hole pairs are formed and the excitation-density dependence of the blue PL intensity and dynamics deviates from that expected from the simple rate equation model because of electron-density distribution between the lower-energy direct and the higher-energy indirect conduction bands. At present, we consider that the electrons in higher-energy indirect band immediately recombine with photoexcited holes through nonradiative Auger recombination, and then the saturation of the blue PL intensity occurs under extremely high-density excitation.

Since the initial PL intensity of direct excitons (peak A) is proportional to the initial photoexcited electron density in the lower-energy direct conduction band (N_L), we plotted the initial PL intensity and the decay time of broad blue PL as functions of the exciton PL (peak A) intensity in Fig. 5. The initial PL intensity shows quadratic dependence on the carrier density in the direct band. The decay time is almost constant in the low-carrier-density region, and it shows N_L^{-2}

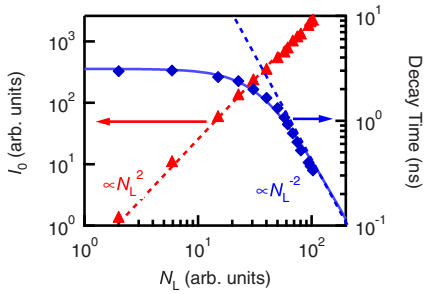

FIG. 5. (Color online) Initial PL intensity and decay time at 8 K as functions of the exciton PL (peak A) intensity (=electron density in the lower-energy direct conduction band, N_L).

dependence in the high-carrier-density region. The solid curve shows fitting result by using $t_{1/e}=1/(2A+2CN_L^2)$, where we neglected B coefficient in Eq. (1a) because of low PL efficiency. The fitting result reproduces the experimental results closely. Therefore, we conclude that the excitation-density dependence of the broad PL in rutile is determined by the electron density in the direct conduction band at low temperatures. The PL behavior is well explained by the simple model involving single-carrier trapping, bimolecular recombination, and Auger recombination processes. At room temperature, the PL behavior is strongly influenced by thermal distribution between the lower-energy direct and the higher-energy indirect conduction bands.

Finally, we comment on the origin of the broad PL band. Based on time-resolved PL measurements, we confirmed that the spectrum shape of the broad PL band is time and excitation-density independent, which means that the origin of the broad PL is not electron-hole plasmas. Actually, the excitation density in this study ($<6\times10^{20}$ cm^{-3}) is smaller than the exciton Mott density in rutile ($n_c\sim10^{21}$ cm^{-3}). The large Stokes shift and spectral width of the blue PL indicates that the initial state of the PL is a low-energy localized state rather than a band-edge delocalized state. Because only a free exciton PL is observed under low-density photoexcitation at low temperatures, the initial photocarriers exist in the free band-edge state rather than self-trapped state[28] (such as a self-trapped exciton or a polaron). At present, we consider that the localized states are induced by defects or unintentional impurities. In addition, quadratic dependence on the excitation density shows that the two-body inelastic scattering such as carrier-carrier or exciton-exciton scattering occurs during the luminescence process. Thus it is likely that the free photocarriers initially produced by photoexcitation are scattered to low-energy localized states through two-body collisions and then recombine radiatively. This recombination process is analogous to P-line emission in highly photoexcited semiconductors.[29] We conclude that nonlinear carrier recombination processes determine the blue PL spectrum and dynamics.

In conclusion, we discovered blue PL in nondoped rutile TiO_2 single crystals under high-density photoexcitation using a pulsed laser. A similar PL band is observed in electron-doped rutile even under weak cw excitation. The blue PL in nondoped and electron-doped rutile is related to high-density carriers in the samples. By considering the nearly degenerate conduction bands of rutile, we revealed that the blue PL dynamics is determined by the electron density in the lower-energy conduction band. The PL decay dynamics is well explained by the simple model involving two-body radiative recombination and three-body Auger recombination processes. Our findings provide a deep understanding of the carrier recombination process of TiO_2 crystals and photocatalytic reactions and solar-energy conversions in TiO_2-based devices.

Part of this work was supported by a Grant-in-Aid for Scientific Research on Innovative Areas "Optical Science of Dynamically Correlated Electrons" (Grant No. 20104006) of the Ministry of Education, Culture, Sports, Science and Technology (MEXT), Japan.

*Corresponding author; kanemitu@scl.kyoto-u.ac.jp

[1] R. R. Hasiguti and E. Yagi, Phys. Rev. B **49**, 7251 (1994).
[2] N. A. Deskins and M. Dupuis, Phys. Rev. B **75**, 195212 (2007).
[3] B. J. Morgan and G. W. Watson, Phys. Rev. B **80**, 233102 (2009).
[4] A. Fujishima and K. Honda, Nature (London) **238**, 37 (1972).
[5] Y. Furubayashi *et al.*, Appl. Phys. Lett. **86**, 252101 (2005).
[6] B. O'Regan and M. Grätzel, Nature (London) **353**, 737 (1991).
[7] C. Colbeau-Justin *et al.*, J. Mater. Sci. **38**, 2429 (2003).
[8] R. Katoh *et al.*, Chem. Phys. Lett. **461**, 238 (2008).
[9] E. Hendry *et al.*, Phys. Rev. B **69**, 081101 (2004).
[10] A. Furube *et al.*, J. Phys. Chem. B, **103**(16), 3120 (1999).
[11] A. K. Ghosh *et al.*, Phys. Rev. B **8**, 4842 (1973).
[12] P. T. Landsberg, *Recombination in Semiconductors* (Cambridge University Press, Cambridge, 1991).
[13] P. T. Landsberg, Appl. Phys. Lett. **50**, 745 (1987).
[14] H. Yasuda and Y. Kanemitsu, Phys. Rev. B **77**, 193202 (2008).
[15] G. E. Jellison, Jr. *et al.*, Opt. Lett. **22**, 1808 (1997).
[16] Y. Yamada *et al.*, Appl. Phys. Lett. **95**, 121112 (2009).
[17] Y. Yamada *et al.*, Phys. Rev. Lett. **102**, 247401 (2009).
[18] J. Pascual *et al.*, Phys. Rev. B **18**, 5606 (1978).
[19] A. Amtout and R. Leonelli, Phys. Rev. B **51**, 6842 (1995).
[20] R. V. Kasowski and R. H. Tait, Phys. Rev. B **20**, 5168 (1979).
[21] M. A. Khan *et al.*, J. Phys.: Condens. Matter **3**, 1763 (1991).
[22] G. A. Acket and J. Volger, Physica (Amsterdam) **32**, 1680 (1966).
[23] B. Poumellec *et al.*, J. Phys.: Condens. Matter **3**, 8195 (1991).
[24] J. H. Becker and W. R. Hosler, Phys. Rev. **137**, A1872 (1965).
[25] E. Yagi *et al.*, Phys. Rev. B **54**, 7945 (1996).
[26] H. P. R. Frederikse, J. Appl. Phys. **32**, 2211 (1961).
[27] S. D. Mo and W. Y. Ching, Phys. Rev. B **51**, 13023 (1995).
[28] Y. Toyozawa, *Optical Processes in Solids* (Cambridge University Press, Cambridge, 2003).
[29] C. F. Klingshirn, *Semiconductor Optics*, 3rd ed. (Springer, Berlin, 2007).